

## X-ray and Optical Monitoring of State Transitions in MAXI J1820+070

MEGUMI SHIDATSU,<sup>1</sup> SATOSHI NAKAHIRA,<sup>2</sup> KATSUHIRO L. MURATA,<sup>3</sup> RYO ADACHI,<sup>3</sup> NOBUYUKI KAWAI,<sup>3</sup> YOSHIHIRO UEDA,<sup>4</sup>  
AND HITOSHI NEGORO<sup>5</sup>

<sup>1</sup>*Department of Physics, Ehime University, 2-5, Bunkyocho, Matsuyama, Ehime 790-8577, Japan*

<sup>2</sup>*High Energy Astrophysics Laboratory, RIKEN, 2-1, Hirosawa, Wako, Saitama 351-0198, Japan*

<sup>3</sup>*Department of Physics, Tokyo Institute of Technology, 2-12-1 Ookayama, Meguro-ku, Tokyo 152-8551, Japan*

<sup>4</sup>*Department of Astronomy, Kyoto University, Kitashirakawa-Oiwake-cho, Sakyo-ku, Kyoto, Kyoto 606-8502, Japan*

<sup>5</sup>*Department of Physics, Nihon University, 1-8-14 Kanda-Surugadai, Chiyoda-ku, Tokyo 101-8308, Japan*

### ABSTRACT

We report results from the X-ray and optical monitoring of the black hole candidate MAXI J1820+070 (=ASSASN-18ey) over the entire period of its outburst from March to October 2018. In this outburst, the source exhibited two sets of “fast rise and slow decay”-type long-term flux variations. We found that the 1–100 keV luminosities at two peaks were almost the same, although a significant spectral softening was only seen in the second flux rise. This confirms that the state transition from the low/hard state to the high/soft state is not determined by the mass accretion rate alone. The X-ray spectrum was reproduced with the disk blackbody emission and its Comptonization, and the long-term spectral variations seen in this outburst were consistent with a disk truncation model. The Comptonization component, with a photon index of 1.5–1.9 and electron temperature of  $\gtrsim 40$  keV, was dominant during the low/hard state periods, and its contribution rapidly decreased (increased) during the spectral softening (hardening). During the high/soft state period, in which the X-ray spectrum became dominated by the disk blackbody component, the inner disk radius was almost constant, suggesting that the standard disk was present down to the inner most stable circular orbit. The long-term evolution of optical and X-ray luminosities and their correlation suggest that the jets substantially contributed to the optical emission in the low/hard state, while they are quenched and the outer disk emission dominated the optical flux in the intermediate state and the high/soft state.

**Keywords:** X-rays: individual (MAXI J1820+070) — X-rays: binaries — accretion, accretion disks — black hole physics

### 1. INTRODUCTION

The Galactic black hole candidate MAXI J1820+020/ASASSN-18ey, discovered in optical by the All-Sky Automated Survey for SuperNovae (ASSAS-SN) project (Shappee et al. 2014) on 2018 March 6 (Tucker et al. 2018) and in X-rays with *MAXI* (Matsuoka et al. 2009) on 2018 March 11 (Kawamuro et al. 2018a), has been an ideal target to probe black hole accretion flows and jets over a wide range of mass accretion rates. Thanks to its relatively small distance ( $3 \pm 1$  kpc, Gandhi et al. 2018b) and low Galactic extinction ( $N_{\text{H}} = 1.5 \times 10^{21} \text{ cm}^{-2}$ , Uttley et al. 2018), the source has been intensively observed at various wavelengths, with dif-

ferent methods (photometry, spectroscopy, and polarimetry), and on various time resolutions, from ms to  $\gtrsim \text{day}$  (Kennea et al. 2018; Kennea & Siegel 2018; Kennea 2018; Baglio et al. 2018; Bright et al. 2018a; Littlefield 2018; Veledina et al. 2018; Uttley et al. 2018; Bahramian et al. 2018; Garnavich & Littlefield 2018; Sako et al. 2018; Del Santo & Segreto 2018; Paice et al. 2018; Gandhi et al. 2018a; Trushkin et al. 2018, and many other reports in the Astronomer’s Telegram).

Since its discovery, the source stayed in the low/hard state for more than 3 months, and then exhibited a rapid X-ray spectral softening in 2018 July (Homan et al. 2018a). This indicates that the source made the state transition from the so-called low/hard state, in which a strong hard X-ray component is observed in the X-ray spectrum, to the high/soft state, where the soft X-ray emission from the standard accretion disk

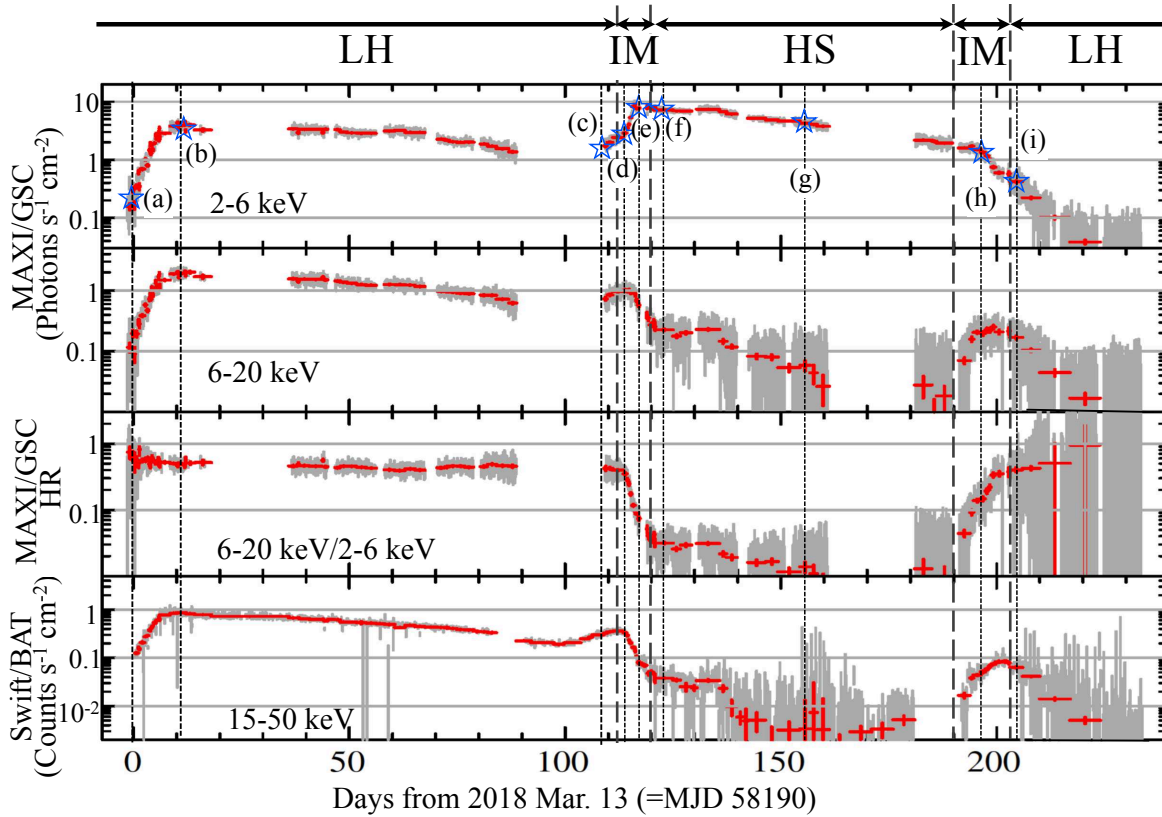


**Figure 1.** *MAXI*/GSC light curves of MAXI J1820+070 in 2–6 keV, 6–20 keV, their hardness ratio, and *Swift*/BAT light curve in 15–50 keV downloaded from the “BAT Transient Monitor” website (Krimm et al. 2013, <http://swift.gsfc.nasa.gov/docs/swift/results/transients>), from top to bottom. The grey and red points show the data with orbital time bins ( $\sim 92$  min) and the binned data, respectively. The error bars indicate  $1\sigma$  statistical errors. The periods “LH”, “IM”, “HS” represent the low/hard, intermediate, and high/soft state periods, respectively. The spectra in the bin (a)–(i) indicated with stars and thin vertical lines are plotted in Fig. 3.

(Shakura & Sunyaev 1973) dominates the X-ray flux. The source exhibited strong radio flares at the beginning of the transition (Bright et al. 2018b). During the transition, the radio to infrared flux decreased, suggesting quenching of the jet (Tetarenko et al. 2018; Casella et al. 2018). By contrast, the optical flux behaved in an opposite way (Tucker et al. 2018). In September, an X-ray spectral hardening was observed, indicating that the source returned to the low/hard state (Negoro et al. 2018; Motta et al. 2018; Homan et al. 2018b).

In Shidatsu et al. (2018) (hereafter S18), we studied the X-ray properties of MAXI J1820+070 using the *MAXI* and *Swift* (Gehrels et al. 2004) data obtained during the low/hard state before the state transition in July. The X-ray spectrum in this period was well explained by Comptonization of soft X-ray photons from the standard disk, in the hot ( $\gtrsim$  several ten keV), radiatively inefficient inner flow or the corona above the disk. We also analyzed a simultaneous multi-wavelength spectral energy distribution taken in late March and found that the synchrotron emission from the jet was likely to

contribute to the optical and near-infrared wavelengths, whereas in the X-ray band, its contribution, as well as the contributions of synchrotron self-Comptonization and external Comptonization, were likely to be negligible.

In this article, we investigate the long-term X-ray spectral evolution over the entire outburst from March to October, using the *MAXI*/Gas Slit Camera (GSC) and *Swift*/Burst Alert Telescope (BAT) data. We also combine the optical photometric data acquired with the MITSuME 50 cm telescope in Akeno Observatory, to study long-term optical flux evolution and correlation with the X-ray flux. We adopt the solar abundance table given by Wilms et al. (2000) for the spectral analysis described below. Errors represent the 90% confidence ranges for one parameter, unless otherwise stated.

## 2. X-RAY DATA REDUCTION AND ANALYSIS

We reduced the *MAXI*/GSC event data and *Swift*/BAT survey data from 2018 March to October, utilizing the *MAXI* analysis tools (Nakahira et al. 2013) and the HEASoft version 6.23, and produced the light curves

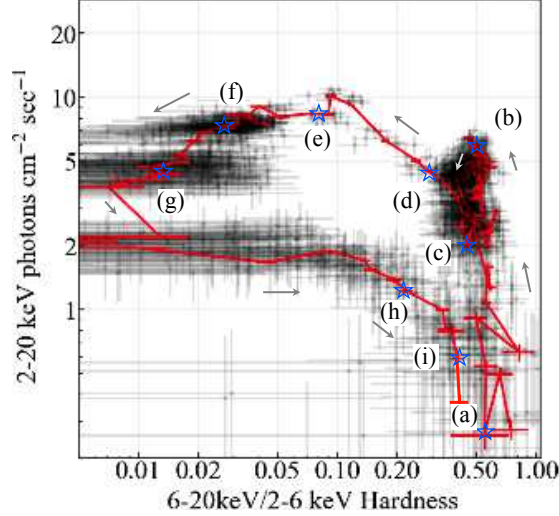


**Figure 2.** Hardness intensity diagram of MAXI J1820+070, created from the MAXI data in Fig. 1. The error bars indicate  $1\sigma$  statistical errors.

and spectra of MAXI J1820+070. We adopted the same procedures of the data reduction as those in S18.

### 2.1. Light Curves and Hardness Ratio

Figure 1 shows the *MAXI*/GSC 2–6 keV and 6–20 keV light curves of MAXI J1820+070, and the *Swift*/BAT light curve in 15–50 keV during the 2018 outburst, with a time bin size of their orbital periods ( $\sim 92$  minutes; grey points). The hardness ratio (HR) calculated from these two *MAXI* light curves is also plotted. Using the MAXI data in Fig. 1, we have also plotted the hardness intensity diagram (HID) of MAXI J1820+070 in Figure 2. To improve statistics, we combined the GSC data taken in each 1–85 adjacent orbits with similar fluxes into one bin (red points in Fig. 1).

The source showed a rapid flux rise and then a slower decay in all energy bands, in the first  $\sim 3$  months after the discovery on 2018 March 11. In this period, the HR was kept almost constant. A re-brightening in the 15–50 keV band was detected with the *Swift*/BAT in the middle of June (MJD  $\sim 58290$ ), whereas the soft X-ray data could not be obtained with the *MAXI* from the beginning to the end of June, because the source was out of its field of view. In early July, *MAXI* detected a rapid increase of the soft X-ray flux in 2–6 keV, to the peak level of  $\sim 10$  photons  $\text{s}^{-1} \text{cm}^{-2}$ , corresponding to  $\sim 4$  Crab. Meanwhile, the hard X-ray flux above 6 keV decreased rapidly a few days before the soft X-ray peak, and the HR thereby dropped.

Since the second flux peak, the soft X-ray flux below 6 keV has been decreasing gradually, whereas the harder X-ray flux increased again from late September to the beginning of October (MJD 58380–58393). Conse-

quently, the HR increased again to the initial level before the re-brightening in June to July. The overall evolution of the fluxes and HR provided a counter-clockwise track in the HID, like typical Galactic transient black hole binaries in their outburst.

Considering the behavior of the HR, we classified the whole outburst period into the canonical three spectral states of black hole X-ray binaries (e.g., Done et al. 2007, for details): the low/hard state, the high/soft state, and the intermediate state (which is the transitional state between the former two states).

**low/hard state:** until MJD 58303.5 and from MJD 58393.0, in which the HR was at the highest level,  $\gtrsim 0.4$ .

**intermediate state:** MJD 58303.5–58310.7 and MJD 58380.0–58393.0, in which the HR was rapidly decreasing/increasing between 0.04–0.4.

**high/soft state:** MJD 58310.7–58380.0, in which the HR was lower than  $\sim 0.04$ .

This classification is confirmed to be valid in the following sections, on the basis of the X-ray spectral profile.

### 2.2. Spectral Analysis

We studied X-ray spectral evolution of MAXI J1820+070 using the *MAXI*/GSC and *Swift*/BAT survey data. We produced *MAXI* spectra in the individual bins presented in Fig. 1 as red points. Following S18, we then matched them with the BAT survey spectra of the individual continuous scans. We thus obtained 93 simultaneous *MAXI*/GSC and *Swift*/BAT spectra covering from 2 keV to  $\sim 200$  keV over the whole outburst. We presented 9 representative spectra in Figure 3.

The simultaneous *MAXI*/GSC and *Swift*/BAT spectra were systematically analyzed on XSPEC version 12.10.0. We varied the cross-normalization factor of the BAT data with respect to the GSC data, to take into account an uncertainty in the instrumental cross-calibration and that caused by flux variation due to the slight differences of the observation periods between the *MAXI*/GSC and *Swift*/BAT. We adopted a canonical spectral model for black hole binaries in outbursts: disk blackbody emission and its thermal or non-thermal Comptonization component. The TBabs model (Wilms et al. 2000) was also employed to account for the interstellar absorption. We fixed the equivalent hydrogen column density  $N_{\text{H}}$  at  $1.5 \times 10^{21} \text{ cm}^{-2}$ , which was determined from the data of the *Neutron star Interior Composition Explorer* (NICER, Uttley et al. 2018).

As investigated in S18, before the spectral softening, the source showed a typical spectral profile of black hole

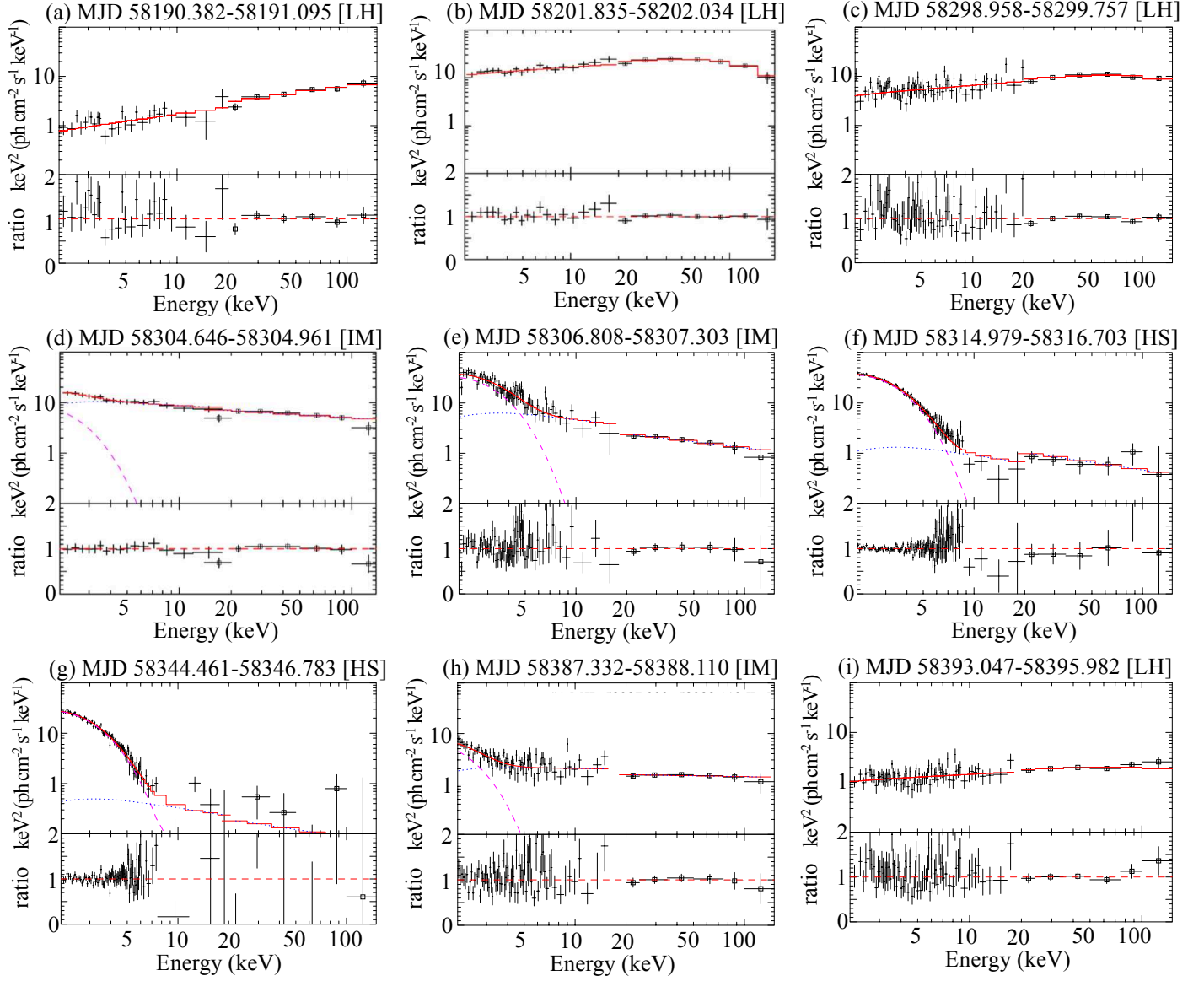


**Figure 3.** Unfolded *MAXI*/GSC (cross) and *Swift*/BAT (open square) spectra, obtained at the epochs (a)–(i) indicated in Fig. 1 and Fig. 2, with their best-fit models (top), and the data versus model ratios (bottom). The unscattered and scattered components are plotted in pink dashed and blue dotted lines, respectively, for the high/soft state and intermediate state spectra.

binaries in the low/hard state: a hard power-law shaped spectrum with a photon index of  $< 2$ , often accompanying an exponential cutoff (see Fig. 3a–c). A similar spectrum was observed after the spectral hardening around MJD 58380–58390 (see Fig. 3i). We applied the same model as S18, `TBabs*nthcomp` to the spectra in these periods. The `nthcomp` model calculates thermal Comptonization spectrum using a photon index and an electron temperature (Zycki et al. 1999). Following S18, the seed spectrum was assumed to be a disk blackbody, with a fixed inner temperature of 0.1 keV, as it cannot be determined with the MAXI+BAT data covering only above 3 keV. The results do not depend on this value,

as all the parameters we obtain remain within their 90% error ranges, even when  $T_{\text{in}} = 0.5$  keV and 0.05 keV are adopted. We ignored the direct disk blackbody component in  $P_{\text{H}}$ .

In the high/soft state, the spectrum of MAXI J1820+070 was dominated by the soft X-rays (see Fig. 3f and g) likely originating in the thermal emission from the standard accretion disk (Shakura & Sunyaev 1973). We used `diskbb` (Mitsuda et al. 1984) to model this component. A weak power-law tail was also often observed above  $\sim 10$  keV, without a significant cutoff. To account for this component, we employed `simpl` (Steiner et al. 2009), assuming the non-thermal Comp-



**Table 2.** Best-fit parameters for the representative spectra

ID <sup>a</sup>	state	model <sup>b,c</sup>	$\Gamma$	$kT_e$	$F_{\text{scat}}$	$kT_{\text{in}}$	$r_{\text{in}}^d$	$\chi^2/\text{dof}$	$F_X^e$
				keV		keV	km		$10^{-8} \text{ erg s}^{-1} \text{ cm}^{-2}$
(a)	low/hard	<b>nthcomp</b>	$1.55 \pm 0.08$	$> 42$	—	0.1 (fixed)	—	29/28	$1.6^{+0.4}_{-0.3}$
(b)	low/hard	<b>nthcomp</b>	$1.72 \pm 0.05$	$41^{+11}_{-7}$	—	0.1 (fixed)	—	27/27	$14 \pm 1$
(c)	low/hard	<b>nthcomp</b>	$1.74^{+0.08}_{-0.07}$	$61^{+139}_{-22}$	—	0.1 (fixed)	—	80/72	$5.0^{+0.6}_{-0.5}$
(d)	intermediate	<b>simpl*diskbb</b>	$2.20 \pm 0.08$	—	$0.4^{+0.1}_{-0.2}$	$0.5 \pm 0.2$	$81^{+190}_{-40}$	18/23	$7.5^{+1.1}_{-0.7}$
(e)	intermediate	<b>simpl*diskbb</b>	$2.4 \pm 0.2$	—	$0.10^{+0.03}_{-0.02}$	$0.67^{+0.06}_{-0.05}$	$67^{+17}_{-12}$	75/80	$10.0^{+0.7}_{-0.8}$
(f)	high/soft	<b>simpl*diskbb</b>	2.5 (fixed)	—	$0.022 \pm 0.004$	$0.70 \pm 0.01$	$61 \pm 2$	118/115	$8.5 \pm 0.2$
(g)	high/soft	<b>simpl*diskbb</b>	2.5 (fixed)	—	$0.01 \pm 0.05$	$0.64 \pm 0.02$	$66 \pm 5$	99/89	$5.9 \pm 0.2$
(h)	intermediate	<b>simpl*diskbb</b>	$2.1 \pm 0.2$	—	$0.12 \pm 0.04$	$0.45 \pm 0.08$	$73^{+61}_{-27}$	88/80	$2.5^{+0.4}_{-0.3}$
(i)	low/hard	<b>nthcomp</b>	$1.83 \pm 0.08$	$> 84$	—	0.1 (fixed)	—	69/77	$1.1 \pm 0.1$

<sup>a</sup>Data IDs in Fig 3.<sup>b</sup>The **TBabs** model was combined for all models, with  $N_H$  of  $1.5 \times 10^{21}$ , to account for the interstellar absorption.<sup>c</sup>The seed spectrum for the Comptonization component was assumed to be a disk blackbody.<sup>d</sup>Inner radius estimated from the total photons of the disk blackbody emission, including the Comptonized photons. A distance and an inclination angle of 3 kpc and  $60^\circ$  are assumed, respectively. The color-temperature correction and the correction of the inner boundary condition are not considered here.<sup>e</sup>Unabsorbed 1–100 keV flux.

tonization of the disk emission as the origin of the hard tail. Thus, the model applied for the high/soft state periods was expressed as **TBabs\*simpl\*diskbb**. The **simpl** model makes a fraction of an input seed spectrum scatter into a power-law component, using a scattered fraction  $F_{\text{scat}}$  and a photon index  $\Gamma$  as the free parameters. We fixed  $\Gamma$  at 2.5, a typical value for the high/soft state (e.g., Ebisawa et al. 1994; McClintock & Remillard 2006), because we were unable to constrain it, due to the low statistics of the *Swift*/BAT data. We extended the energy range over which the model spectrum is calculated on XSPEC, from those in the *MAXI*/GSC and *Swift*/BAT response matrix files to 0.1–500 keV, for accurate calculation of the convolution model **simpl**.

The spectrum changed drastically during the intermediate states, as shown in Fig. 3(c)–(e) and (h). We applied the same model as that used for the spectrum in the high/soft state. **TBabs\*simpl\*diskbb**, varying the photon index. We note that the **simpl** model does not consider the radial dependence of the scattering fraction. This means that it assumes a specific geometry (a disk-like geometry) for the Comptonized region, and its parameters may become unreliable when a different geometry is considered, such as a spherical electron cloud inside a highly truncated standard disk. We have also tested the disk and its thermal Comptoniza-

tion model, **TBabs\*(diskbb+nthcomp)**, linking the inner disk temperatures of **diskbb** and **nthcomp**, and have obtained equally good fit with parameter values similar to **TBabs\*simpl\*diskbb**. The spectral cutoff was not detected significantly and only a lower limit of the electron temperature was obtained ( $kT_e \gtrsim 50$  keV).

These models successfully described the wide-band *MAXI*/GSC and *Swift*/BAT X-ray spectra in the individual states. The best-fit models for the 9 representative spectra and their parameters are presented in Figure 3 and Table 2, respectively. Figure 4 shows the trend of the fit parameters over the entire outburst. As found by S18, the photon index and the electron temperature slightly increased and decreased, respectively, during the flux rise at the beginning of the outburst. In the second flux rise from MJD~58300, the **diskbb** component emerged from the low edge of the *MAXI* energy band and it contributed more to the X-ray spectrum as the source became brighter. In the high/soft state, the total X-ray flux varied by a factor of  $\sim 5$  and the inner disk temperature varied between  $\sim 0.4$  and  $\sim 0.7$ , whereas the inner disk radius was fairly constant at  $\sim 60$  ( $D/3$  kpc) ( $\cos i / \cos 60^\circ$ ) km, where  $D$  and  $i$  are the distance and the inclination angle.

The iron  $K\alpha$  emission line, often seen in other sources during the low/hard state and the intermediate state, was not detected significantly in any of the above spec-

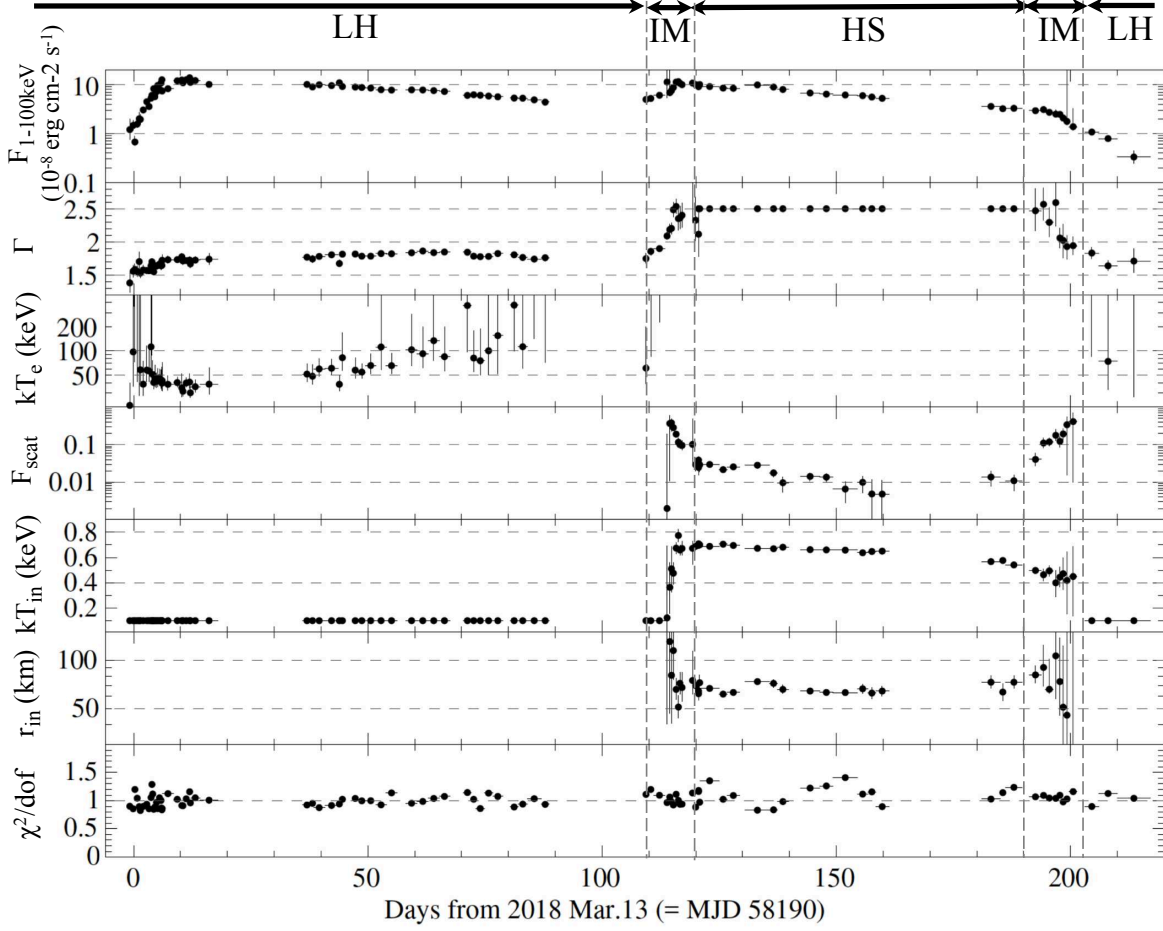


**Figure 4.** Time variations of the parameters in the best-fit models. The unabsorbed 1–100 keV flux (in units of  $10^{-8}$  erg s $^{-1}$  cm $^{-2}$ , estimated by adopting the normalization of the *MAXI*/GSC data), the photon index, the electron temperature (keV), the fraction of the Comptonization component, the inner disk temperature (keV), the inner disk radius (km) estimated by assuming a distance of 3 kpc and an inclination angle of  $60^\circ$ , and the reduced chi-squared, from top to bottom.

tra. This is most likely because of statistics and energy resolution of the *MAXI*/GSC. Fitting the spectrum (b) in Fig. 3 with the `tbabs*nthcomp` model plus a Gaussian component, which represents the iron line, we estimated the upper limit on the equivalent width of the line as  $\sim 300$  eV. This is consistent with the typical values in the low/hard state  $\lesssim 100$  eV (e.g., Makishima et al. 2008; Kolehmainen 2014). In this fit, the line-center energy and the width were fixed to 6.4 keV and 100 eV, respectively, referring to the values obtained in GX 339–4 (Shidatsu et al. 2011b). The results were confirmed to be unaffected, even when the line center energy is changed to 6.9 keV, corresponding to the H-like iron, and when the line width is varied by a factor of 5.

### 3. OPTICAL DATA REDUCTION AND ANALYSIS

Optical photometric observations of MAXI J1820+070 in the  $g'$  band were performed with the MITSuME 50 cm telescope in Akeno Observatory, Yamanashi, Japan (Kotani et al. 2005; Yatsu et al. 2007; Shimokawabe et al.

2008), based on a Target-of-Opportunity program in the Optical and Infrared Synergetic Telescopes for Education and Research (OISTER). We reduced the  $g'$ -band data following standard procedures including bias and dark subtraction, flat fielding, and bad pixel masking, and then performed photometry of MAXI J1820+070 using IRAF. Magnitude calibration was carried out by using the magnitudes of nearby reference stars, which were taken from the UCAC4 catalog (Zacharias et al. 2013). The source was also observed through several different optical and near-IR filters, with telescopes involved in the OISTER. The complete datasets and their analysis will be presented by Adachi et al. (in preparation).

Figure 5 shows the unabsorbed 2–10 keV light curve obtained from the best-fit models in Section 2.2, and the optical  $g'$ -band light curve from the MITSuME telescope. The optical data were dereddened with the reddening factor  $A_{g'} = 0.98$ . This value was obtained by using the extinction law given in Cardelli et al. (1989) and

the reddening factor in the  $V$ -band,  $A_V = 0.84$ , which was derived from the absorption column  $N_H = 1.5 \times 10^{21} \text{ cm}^{-2}$  via the  $N_H$  vs.  $A_V$  relation in [Predehl & Schmitt \(1995\)](#). The errors of the magnitudes include both the statistical photometric errors of MAXI J1820+070 and the systematic errors of the reference star magnitudes (typically  $\sim 0.034$  mag in total). Overall, the optical flux increased (decreased) with increasing (decreasing) X-ray flux, although a weak optical re-brightening took place just after the soft-to-hard transition during the X-ray decay (MJD  $\sim 58400$ ), as was reported by [Baglio et al. \(2018\)](#). A remarkable point is that the  $g'$ -band flux at the first peak on MJD  $\sim 58202$  is higher than that at the second peak on MJD  $\sim 58306$  by  $\sim 1$  mag (by a factor of  $\sim 2.5$  in the flux unit), whereas the X-ray flux at the first peak is slightly lower than that at the second peak.

To investigate a flux correlation between the X-ray and optical bands, we also plotted the optical vs. X-ray luminosity diagram in Figure 6 using the simultaneous data in Fig. 5. The optical magnitudes were converted to fluxes, and multiplied by the central frequency of the  $g'$ -band filter,  $\nu = 6.25 \times 10^{14} \text{ Hz}$ , following [Russell et al. \(2006\)](#), to obtain the fluxes in the  $\nu F_\nu$  units. Using these extinction/absorption-corrected optical and X-ray fluxes, we estimated the optical and X-ray luminosities,  $L_{\text{opt}}$  and  $L_{2-10 \text{ keV}}$ , respectively, assuming an isotropic radiation at a distance of 3 kpc. As is noticed in this figure, the data points are more highly scattered and  $L_{\text{opt}}$  with respect to  $L_{2-10 \text{ keV}}$  is somewhat higher in the low/hard state than in the intermediate state and the high/soft states. The data points in the latter two states can be described with a power-law function. Fitting the data of the two states in Fig. 6 together, we obtained the best-fit model of  $L_{\text{opt}} \propto L_{2-10 \text{ keV}}^{0.51 \pm 0.03}$ .

#### 4. DISCUSSION

##### 4.1. Interpretation of the Long-term X-ray Evolution

We have monitored MAXI J1820+070 in 2–200 keV during its outburst using *MAXI/GSC* and *Swift/BAT*. In the soft X-ray band below 6 keV, it showed two “rapid rise and slow decay”-type long-term flux evolutions (hereafter we call them as the first/second sub-outbursts). This profile is often seen in X-ray light curves of transient black hole X-ray binaries. The two big sub-outbursts suggest that, in this outburst, the source exhibited two discrete increases in its mass accretion rate through the disk. Re-flares in the outburst decay have been observed in many other black hole X-ray binaries, and they usually occur after 50–100 days from the first flux peak (e.g., [Chen et al. 1993](#); [Nakahira et al. 2014](#)). This interval is similar to that of the two sub-outbursts in MAXI J1820+070.

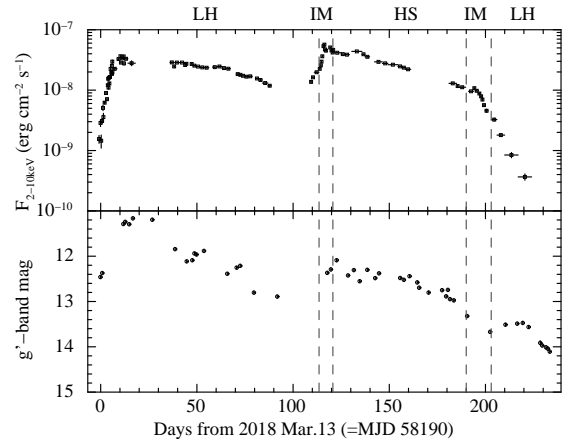


**Figure 5.** X-ray 2–10 keV (top) and optical  $g'$ -band (bottom) light curves of MAXI J1820+070. The X-ray light curve was obtained from the best-fit model in Section 2.2 and corrected for the interstellar absorption. The optical magnitudes were corrected for reddening and are expressed in the AB system. The error bars of the optical light curves include both the statistical photometric errors of MAXI J1820+070 and the systematic errors of the reference star magnitudes ( $\sim 0.034$  mag in total).

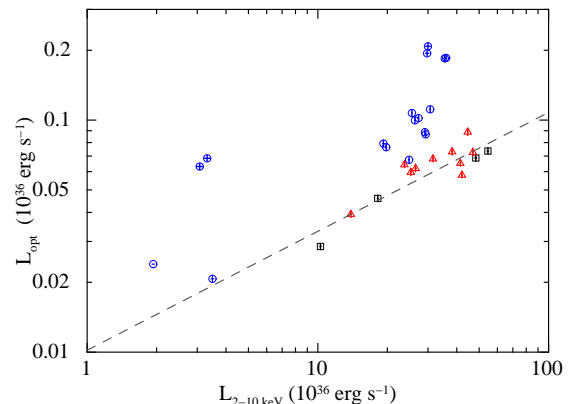


**Figure 6.** Correlation of X-ray and optical luminosities of MAXI J1820+070. Blue circles, black squares, and red triangles indicate the data taken in the low/hard state, the intermediate state, and the high/soft state, respectively. The dashed lines are the best-fit power-law function for the data points in the latter two states,  $L_{\text{opt}} \propto L_{2-10 \text{ keV}}^{0.51 \pm 0.03}$ .

Such re-flares were often interpreted by the enhancement of the mass accretion rate from the donor star, which was inflated due to the X-ray irradiation ([Chen et al. 1993](#); [Mineshige 1994](#)). This could also explain the second sub-outburst of MAXI J1820+070, as was discussed in S18. However, the re-flares in other sources are usually much weaker than their main outbursts, having  $\sim 1$  order of magnitude lower peak luminosities than those of the main outbursts. Why such a strong re-brightening took place in MAXI J1820+070

is an open question, but maybe it is because the source stayed in the low/hard state during the first sub-outbursts, and the strong hard X-rays heated the companion star more efficiently than other sources with re-flares, which often show state transitions in their main outbursts.

The HR was almost constant at a high level during the first sub-outburst, whereas its rapid decrease was observed in the second sub-outburst. This indicates that the state transition from the low/hard state to the high/soft state (the hard-to-soft transition) took place only in the second sub-outburst. Interestingly, the 1–100 keV fluxes were almost the same (different only by  $\sim 10\%$ ) at the flux peaks in the two sub-outbursts. If the radiation efficiency was constant during the outburst, this suggests that the mass accretion rates were the same in the two peaks, and that the hard-to-soft transition is not determined the mass accretion rate alone. We note that, however, in reality, the radiation efficiency most likely varies, depending on the properties of the accretion flow and outflows (e.g., Malzac et al. 2004; Kato et al. 2008, and references therein). Hence, the same X-ray luminosity does not necessarily mean the same mass accretion rate, and it is difficult to completely rule out, using our results alone, the possibility that the mass accretion rate at the beginning of the hard-to-soft transition was higher than that at the first X-ray peak.

More direct evidence that something other than the mass accretion rate plays a role to trigger the hard-to-soft transitions, has been found in previous observations. As was observed in other sources such as GX 339–4, the hard-to-soft transitions actually took place at different luminosities in different outbursts of the same sources (e.g., Dunn et al. 2008). What made the difference in the two sub-outbursts of MAXI J1820+070 is still unclear, but it may be related to the magnetic fields in the inner disk region, considering previous theoretical studies of the accretion flows in the hard-to-soft transition (Machida et al. 2006; Begelman & Armitage 2014). Perhaps, in the first sub-outburst, strong magnetic fields were present in the inner disk region for some unknown reasons, and prevented from developing the standard disk inwards.

Although the low/hard state period before the hard-to-soft transition was unusually long, the combination of two sub-outburst provided a normal “q”-shaped track in the HID, like other black hole binaries. The hysteretic behavior in the HID, where the hard-to-soft transition occurs at higher luminosity than that of the transition from the high/soft state back to the low/hard state (the soft-to-hard transition), is seen not only in black hole binaries but also neutron star low

mass X-ray binaries (Muñoz-Darias et al. 2014). However, MAXI J1820+070 is unlikely to harbor a neutron star. Typical soft X-ray spectra of neutron star low-mass X-ray binaries at high luminosities show a thermal emission component with a temperature of  $\sim 1$  keV and a comparably strong Comptonization component located at slightly higher energies than the thermal component, and these two components are considered to originate in the blackbody emission of the neutron star surface and a Comptonized disk emission (Mitsuda et al. 1989), respectively, or the disk blackbody emission and a Comptonized neutron star blackbody emission (Church & Balucinska-Church 1995), respectively. By contrast, all the high/soft-state spectra of MAXI J1820+070 below 10 keV were successfully described by a single disk blackbody model with  $T_{\text{in}} \lesssim 1$  keV. We have confirmed that the fit of the spectrum (f) in Fig. 3 is not improved when `nthcomp` with  $kT_e = 5$  keV (a typical value for the Comptonization component of neutron star X-ray binaries) is added to the `simpl*diskbb` model. These results support that its compact object is not a neutron star but a black hole.

The all-time monitoring and the wide coverage provided by the combination of the *MAXI*/GSC and *Swift*/BAT, have enabled us to simultaneously determine the levels of the disk and Comptonization components in the X-ray spectrum of MAXI J1820+070, and study their long-term variations in the outburst. We discuss the evolution of the structure of the accretion flow, based on the results from our spectral analysis.

In the low/hard state, the spectrum was well described with a thermal Comptonization component with  $\Gamma < 2.0$  and  $kT_e \gtrsim 40$  keV. We detected a gradual increase of  $\Gamma$  and decrease of  $kT_e$  during the rapid flux increase in the first sub-outburst (see Tab. 2 and Fig. 4). As discussed in S18, this could be explained by the disk truncation model, in which the standard disk is truncated in the beginning of the outburst, and it develops inward as the X-ray flux increases (e.g., Done et al. 2007, for more details). The seed photons for Compton scattering increases as the standard disk extends inward, which would cause a more effective cooling of the hot inner flow or corona.

In the intermediate state, where the spectral softening/hardening took place, the inner disk temperature rapidly increased as the total X-ray flux increased, while the fraction of the Comptonization component in the total X-ray flux dropped and the photon index increased up to  $\sim 2.5$ . The rapid change of the X-ray spectrum is typical of black hole X-ray binaries in the intermediate state. In this phase,  $r_{\text{in}}$  was not well constrained, due to uncertainties in the inner disk temperature and the



normalization of the direct disk component, whose contribution to the total X-ray flux was smaller than that in the high/soft state.

After the hard-to-soft transition, the contribution of the Comptonization component decreased down to less than a few %, a typical value in the high/soft state. During the high/soft state, the inner radius was almost constant at  $r_{\text{in}} \sim 60 (D/3 \text{ kpc}) (\cos i / \cos 60^\circ)^{-1/2} \text{ km}$ , even though the 1–100 keV flux decreased by a factor of  $\sim 5$ . This indicates that the standard disk extended stably down to the innermost stable circular orbit (ISCO) in this period.

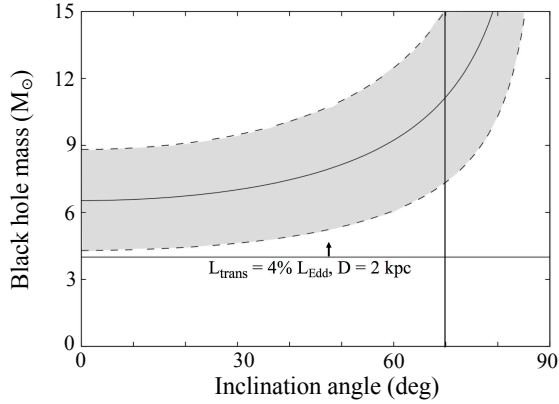


**Figure 7.** Constraints on the black hole mass and the inclination angle of MAXI J1820+070, in the case of a non-spinning black hole. The horizontal and vertical lines present the lower limit of the mass imposed by the luminosity at the soft-to-hard transition, and the lower limit of the inclination angle at which the dips are observed, respectively. The solid curve shows the relations obtained from the constant inner radius in the high/soft state, and the dashed ones separating the shadowed region are its upper/lower limits considering the errors of the inner disk radius and the distance.

#### 4.2. Estimation of System Parameters

We have attempted to constrain the black hole mass using the results of our spectral analysis. Maccarone (2003) suggested that the soft-to-hard transition occurs at 1–4 % Eddington luminosity ( $L_{\text{Edd}}$ ). The 0.01–100 keV flux at the beginning of the soft-to-hard transition is estimated to be  $\sim 5 \times 10^{-8} \text{ erg cm}^{-2} \text{ s}^{-1}$  from the best-fit model, which can be converted to a luminosity of  $\sim 5 \times 10^{37} (D/3 \text{ kpc})^2 \text{ erg s}^{-1}$ , if an isotropic emission is assumed. Considering the uncertainties in the transition luminosity and the distance ( $\approx 3 \pm 1 \text{ kpc}$ ; Gandhi et al. 2018b), the lower limit of the black hole mass ( $M_{\text{BH}}$ ) of MAXI J1820+070 is calculated as  $4 M_{\odot}$ , when  $D = 2 \text{ kpc}$  and the transition luminosity of 4%  $L_{\text{Edd}}$  are adopted. This value justifies that the source has a black hole accretor.

Another constraint is given from the inner disk radius in the high/soft state, which is considered to be identical to the radius of the ISCO. We derive  $r_{\text{in}} = 66.0 \pm 0.8 (D/3 \text{ kpc}) (\cos i / \cos 60^\circ)^{-1/2} \text{ km}$  as a weighted average of the inner radii estimated in the high/soft state. Applying the combined correction factor of 1.18, for the stress-free boundary condition and the color-temperature correction (see e.g., Kubota et al. 1998), we obtain  $R_{\text{in}} = 77.9 \pm 1.0 (D/3 \text{ kpc}) (\cos i / \cos 60^\circ)^{-1/2} \text{ km}$ . In Figure 7, we plot the constraint obtained by equating this radius to that of the ISCO, as a shaded region on the  $M_{\text{BH}}$  versus  $i$  plane. Here, we have assumed a non-rotating black hole, in which case the radius of the ISCO is  $6 GM_{\text{BH}}/c^2$  (where  $G$  and  $c$  are the gravitational constant and the light speed, respectively).

In the beginning of the outburst, *NICER* detected a strong absorption dips (Homan et al. 2018c), which are often seen in X-ray binaries with high inclination angles above  $\sim 70^\circ$  (e.g., Boirin & Parmar 2003; Homan et al. 2005, and references therein). If MAXI J1820+070 has a high inclination angle similar to other dipping sources, a lower limit of  $M_{\text{BH}}$ ,  $\sim 7 M_{\odot}$ , is obtained from Fig. 7. The origin of the dips in MAXI J1820+070 is not yet fully understood, however; the dips have not been detected after the flux peak in the first sub-outburst. Also, ionized absorption lines from disk winds, also often observed in high inclination sources, have never been detected in the outburst. The allowed range of  $M_{\text{BH}}$  becomes lower if the source has a smaller inclination angle than other X-ray binaries with dips and ionized absorption lines.

If the black hole of MAXI J1820+070 is a Kerr (rotating) black hole, the  $M_{\text{BH}}$  values become larger (by up to a few to several times in the case of the maximum spin) than those in the zero-spin case, primarily because the ISCO radius decreases from  $6 GM_{\text{BH}}/c^2$  up to  $\sim 1 GM_{\text{BH}}/c^2$ , as the black hole spin becomes higher (see Davis et al. 2011 for more detailed discussion and Davis et al. 2011; Shidatsu et al. 2011a; Wang et al. 2018 for comparisons of the constraints on  $M_{\text{BH}}$  among different spin parameters). In the case of a highly spinning black hole, the strong relativistic effects, including gravitational redshift and light bending in the vicinity of the black hole, and the Doppler beaming due to the disk rotation, modifies the observed disk spectrum from that obtained with the simple `diskbb` model, and hence disk emission models considering these effects, instead of the simple multi-color disk model, must be employed to describe the spectra and to determine  $M_{\text{BH}}$  accurately. However, the *MAXI* spectra do not have statistics and soft X-ray coverage sufficient to apply such relativistic disk emission models. For further studies, we need data from soft X-ray detectors like *NICER*, with high sen-

sitivity but free from the pile-up effects, This is beyond the scope of this work and we leave it as a future work.

Also, the common transition luminosity estimated by Maccarone (2003) may not always be applicable; an exception has recently been found in the outburst of MAXI J1535–571 (Nakahira et al. 2018), which stayed in the high/soft state even after the X-ray flux decreased  $\sim 3$  orders of magnitude from the luminosity of the hard-to-soft transition. To derive more accurate  $M_{\text{BH}}$  and to test the argument on the transition luminosity, determination of the mass function of MAXI J1820+070 is required via optical spectroscopy in the quiescence phase.

#### 4.3. Optical and X-ray Correlation

In most of the outburst period, the optical flux increased/decreased with the X-ray flux rise/decay, although in the optical band, the second sub-outburst was weaker than the first sub-outburst, unlike those in the X-ray band; in 2–10 keV, the second peak flux was twice higher than that of the first peak. Consequently, the  $L_{\text{opt}}/L_{2-10 \text{ keV}}$  ratio in the intermediate state and the high/soft state is relatively small compared with that in  $P_{\text{H}}$  (see Fig. 6). Similar trend was found in other BHBs (Russell et al. 2006). The difference in the  $L_{\text{opt}}/L_{2-10 \text{ keV}}$  value can be explained by the contribution of the jet in the optical band during the low/hard state. Indeed, S18 found that the jet emission can substantially contribute to the optical flux but not significantly to the X-ray flux of MAXI J1820+070 during the low/hard state. A smaller  $L_{\text{opt}}/L_{2-10 \text{ keV}}$  value would be obtained if the jet is suppressed in the other states, as suggested by Tetarenko et al. (2018); Casella et al. (2018). We note, however, that the synchrotron emission from a magnetized hot inner accretion flow could also considerably contribute to the optical flux and its variation in the low/hard state, as suggested by Veledina et al. (2018). It is difficult to separate the contributions of the jets and the hot inflow, because they can have similar SED profiles and variability properties (Veledina et al. 2013, 2018).

We have found a tight correlation between the X-ray and optical luminosities in the intermediate state and the high/soft state, which is well reproduced by a power-law model as  $L_{\text{opt}} \propto L_{2-10 \text{ keV}}^{0.51 \pm 0.03}$ , whereas the data points in the low/hard state are strongly scattered. Considering that our optical and X-ray observations were not exactly simultaneous, the scatter in the low/hard state could be produced by the strong flux variations in both optical and X-ray bands on timescales of  $< \text{day}$ , which are likely to originate in synchrotron radiation from the jets or the hot inflow, and Comptonization of

the disk photons in the hot inflow/corona, respectively (e.g., Gandhi et al. 2018a; Tucker et al. 2018; S18). By contrast, appearance of the strong X-ray-optical correlation in the intermediate state and the high/soft state would indicate the suppression of such variability in these states, and this could be explained if the jets were quenched and the standard disk was developed close to the ISCO, replacing the hot inner flow.

When the variable emission components are suppressed, the blackbody emission from the companion star, and/or the reprocessed emission from the outer disk irradiated by strong X-rays, are the possible origins of the optical flux. The former possibility is unlikely in MAXI J1820+070, because its optical magnitude in quiescence was found to be  $\gtrsim 18$  mag, much lower than those during the outburst (S18). Hence, the observed correlation in the intermediate state and the high/soft state would be produced by variation of the disk emission. If the optical band is located in the Rayleigh-Jeans (RJ) part of the disk spectrum,  $L_{\text{opt}}$  should be proportional to  $L_{\text{X}}^{1/4}$ . If it is located in the flat part of the irradiated disk spectrum, which is produced at higher frequencies than the RJ part by the reprocessing of the X-rays (Gierliński et al. 2009),  $L_{\text{opt}} \propto L_{\text{X}}$  is realized (e.g., Coriat et al. 2009; Shidatsu et al. 2011b). The index of the correlation that we obtained,  $0.51 \pm 0.03$ , is larger than that expected in the RJ part and smaller than that of the flatter part, and therefore the  $g'$ -band frequency of MAXI J1820+070 may correspond to the transition region between the RJ and flat parts, somewhere around the peak frequency of the blackbody emission of the outer disk edge.

If the above discussion is correct, the  $g'$  band approximately corresponds to the peak of the blackbody emission from the irradiated outer disk edge, and this gives the outer disk temperature,  $T_{\text{out,eff}} \sim 0.1 \text{ eV}$ . The total flux generated at the outer edge,  $\sigma T_{\text{out,eff}}^4$  (where  $\sigma$  is the Stefan-Boltzmann constant) is determined by the sum of the intrinsic disk flux at the outer edge,  $\sigma T_{\text{in}}^4 \left(\frac{R_{\text{out}}}{R_{\text{in}}}\right)^{-3}$  (where  $R_{\text{out}}$  is the outer disk radius), and the illuminating X-ray flux that is thermalized at  $R_{\text{out}}$ . Assuming the irradiated disk model constructed by Gierliński et al. (2009), where the illuminating X-ray flux decreases in proportion to  $r^{-2}$  and a fraction  $f_{\text{out}}$  of it is thermalized, the total flux at  $R_{\text{out}}$  is expressed as

$$\sigma T_{\text{out,eff}}^4 = \sigma T_{\text{in}}^4 \left(\frac{R_{\text{out}}}{R_{\text{in}}}\right)^{-3} + f_{\text{out}} \sigma T_{\text{in}}^4 \left(\frac{R_{\text{out}}}{R_{\text{in}}}\right)^{-2}. \quad (1)$$

In the high/soft state, the second term is usually dominant and  $f_{\text{out}}$  is typically  $\sim 10^{-3}$  (e.g., Gierliński et al. 2009). Adopting  $T_{\text{in}} \sim 0.7 \text{ keV}$ , a typical value of

MAXI J1820+070 in the high/soft state, we obtain  $R_{\text{out}} \sim 10^6 R_{\text{in}} \sim 10^7$  km. Application of this value to the Kepler's third law gives a lower limit on the orbital period,  $\sim 2 ((M_{\text{BH}} + M_c)/10M_{\odot})^{-1/2}$  day, where  $M_c$  is the mass of the companion star. The above calculation is just a rough order-of-magnitude estimation based on some assumptions, and should be tested in the future by e.g., modeling spectral energy distribution from optical to X-ray bands, and measuring orbital modulations of emission/absorption lines through optical spectroscopy.

## 5. SUMMARY

We have studied the nature of MAXI J1820+070 and the evolution of its accretion disk structure, using the *MAXI*/GSC and *Swift*/BAT data obtained in almost the entire period of the 2018 outburst. The behavior in the hardness intensity diagram, the basic properties of the X-ray spectra, and the constraints on accretor's mass obtained from our spectral analysis, indicate that the source is a black hole binary. We found that the outburst is composed of two “fast rise and slow decay”-type flux evolutions, with almost the same total X-ray luminosity at the peaks, although the state transition only took

place in the second flux rise and decay. This implies that the mass accretion rate is not the unique factor to trigger the transition to the high/soft state. The X-ray spectrum was well described with the standard disk emission and its Comptonization, and its long-term variation can be explained in terms of the disk truncation model. The optical-X-ray luminosity correlation suggests that in the low/hard state the optical flux was substantially contributed by emission from the jets, which was likely to be suppressed in the intermediate and high/soft state.

We acknowledge the use of *MAXI* data provided by RIKEN, JAXA and the *MAXI* team, and of public data from the *Swift* data archive. Part of this work was financially supported by Grants-in-Aid for Scientific Research 16K17672 (MS), 17H06362 (NK, YU, HN), and 16K05301 (HN) from the Ministry of Education, Culture, Sports, Science and Technology (MEXT) of Japan. This work was supported by Optical and Near-Infrared Astronomy Inter-University Cooperation Program and the joint research program of the Institute for Cosmic Ray Research (ICRR).

*Facilities:* *MAXI*(GSC), *Swift*(BAT)

## REFERENCES

- Bahramian, A., Strader, J., Dage, K. 2018, ATel #11424  
 Baglio, M. C., Russell, D. M. & Lewis, F. 2018a, ATel #11418  
 Baglio M. C., Russell, D. M., Al Qaissieh, T., et al. 2018a, ATel #12128  
 Begelman, M. C., & Armitage, P., J. 2014, ApJL, 782, 18  
 Berdyugin, A., Beledina, A., Kosenkov., I., et al. 2018, ATel #11445  
 Blandford, R. D., & Königl, A. 1979, ApJ, 23 2, 34  
 Boirin, L., & Parmar, A. N. 2005, A&A, 407, 1079  
 Bright, J., Fender, R. & Motta, S. 2018a, ATel #11420  
 Bright, J., Motta, S., Fender, R., Perrott, Y., & Titterton, D. 2018b, ATel #11827  
 Cardelli, J. A., Clayton, G. C., & Mathis, J. S. 1989, ApJ, 345, 245  
 Casella, P., Testa, V., Russell, D. M., Belloni, T. M., T. J. 2018, ATel #11833  
 Chen, W., Livio, M. & Gehrels, N. 1993, ApJ, 408, 5  
 Church, M. J., & Balucinska-Church, M. 1995, A&A, 300, 44  
 Coriat, M., Corbel, S., Buxton, M. M., et al. 2009, MNRAS, 400, 123  
 Del Santo, M., & Segreto, A. 2018, ATel #11427  
 Davis, S. W., Narayan, R., Zhu, Y., et al. 2011, ApJ, 734, 111  
 Denisenko, D. 2018, ATel #11400  
 Done, C., Gierliński, M., & Kubota, A. 2007, A&A Rv, 15, 1  
 Dunn, R. J. H., Fender, R. P., Körding E. G., Cabanac, C., & Belloni, T. 2008, MNRAS, 387, 545  
 Ebisawa, K., Ogawa, M., Aoki, T., et al. 1994, PASJ, 46, 375  
 Gandhi, P., Paice, J. A., Littlefair, S. P., et al. 2018, ATel #11437  
 Gandhi, P., Rao, A., Johnson, M. A. C., Paice, J. A., & Maccarone, T. J. 2018, ArXiv:1804.11349  
 Garnavich, P., & Littlefield, C. 2018, ATel #11425  
 Gehrels, N., Chincarini, G., Giommi, P., et al. 2004, ApJ, 611, 1005  
 Gierliński, M., Done, C., & Page, K. 2009, MNRAS, 392, 1106  
 Homan, J., Miller, J. M., Wijnands, R., et al. 2005, ApJ, 623, 383  
 Homan, J., Uttley, P., Gendreau, K., et al. 2018a, ATel #11820

- Homan, J., Stevens, A. L., Altamirano, D., et al. 2018b, ATel #12068
- Homan, J., Altamirano, D., Arzoumanian, Z., et al. 2018c, ATel #11576
- Kato, S., Fukue, J., & Mineshige, S. 2008, *Black Hole Accretion Disks-Towards a New Paradigm* (Kyoto: Kyoto Univ. Press)
- Kawamuro, T., Negoro, H., Yoneyama, T., et al. 2018, ATel #11399
- Kennea, J. A., Marshall, F. E., Page, K. L., et al. 2018, ATel #11403
- Kennea, J. A., & Siegel, M. H. 2018, ATel #11404
- Kennea, J. A. 2018, ATel #11406
- Kolehmainen, M., Done, C., & Díaz Trigo, M. 2014, MNRAS, 437, 316
- Kotani, T., Kawai, N., Yanagisawa, K., et al. 2005, *Nuovo Cimento C Geophysics Space Physics C*, 28, 755
- Krimm, H. A., Holland, S. T., Corbet, R. H. D., et al. 2013, Arxiv:1309.0755
- Kubota, A., Tanaka, Y., Makishima, K., et al. 1998, PASJ, 50, 667
- Littlefield, C. 2018, ATel #11421
- Maccarone, T. J. 2003, A&A, 409, 697
- Machida, M., Nakamura, K. E., & Matsumoto, R. 2006, PASJ, 58, 193
- Malzac, J., Merloni, A., Fabian, A. C. 2004, MNRAS, 351, 253
- Matsuoka, M., Kawasaki, K., Ueno, S., et al. 2009, PASJ, 61, 999
- McClintock, J. E., & Remillard, R. A. 2006, in *Compact Stellar X-Ray Sources*, ed. W. H. G., Lewin, & M. van der Klis (Cambridge: Cambridge Univ. Press), 157
- Makishima, K., Takahashi, H., Yamada, S., et al. 2008, PASJ, 60, 585
- Mineshige S. 1994, ApJL, 431, 99
- Mitsuda, K., Inoue, H., Koyama, K., et al. 1984, PASJ, 36, 741
- Mitsuda, K., Inoue, H., Nakamura, N., & Tanaka, Y. 1989, PASJ, 41, 97
- Motta, S. E., Bright, J., & Fender, R. 2018, ATel, #12064
- Muñoz-Darias, T., Fender, R. P., Motta, S. E., & Belloni, T. M. 2014, MNRAS, 443, 3270
- Nakahira, S., Yamaoka, K., Sugizaki, M., et al. 2010, PASJ, 62, L27
- Nakahira, S., Ebisawa, K., Negoro, H., et al. 2013, *Journal of Space Science Informatics*, 2, 29
- Nakahira, S., Negoro, H., Shidatsu, M., et al. 2014, PASJ, 66, 84
- Nakahira, S., Shidatsu, M., Makishima, K., et al. 2018, PASJ, in press
- Negoro, H., Kohama, M., Serino, M., et al. 2016, PASJ, 68, 1
- Negoro, H., Nakajima, M., Sakamaki, A., et al. 2018, ATel, #12057
- Paice, J. A., Gandhi, P., Page, K., et al. 2018, ATel #11432
- Predehl, P., & Schmitt, J. H. M. M. 1995, A&A, 293, 889
- Russell, D. M., Fender, R. P., Hynes, R. I., et al. 2006, MNRAS, 371, 1334
- Sako, S., Ohsawa, R., Ichiki, M., et al. 2018, ATel #11426
- Shakura, N. I., & Sunyaev, R. A. 1973, A&A, 24, 337
- Shappee, B. J., Prieto, J. L., Grupe, D., et al. 2014, ApJ, 788, 48
- Shidatsu, M., Ueda, Y., Nakahira, S., et al. 2011a, pasj, 63, 803
- Shidatsu, M., Ueda, Y., Tazaki, F., et al. 2011b, pasj, 63, 785
- Shidatsu, M., Nakahira, S., Yamada, S., et al. 2018, ApJ, in press (S18)
- Shimokawabe, T., Kawai, N., Kotani, T., et al. 2008, in *American Institute of Physics Conference Series*, Vol. 1000, GAMMA-RAY BURSTS 2007, ed. M. Galassi, D. Palmer, & E. Fenimore, 543–546
- Steiner, J. F., Narayan, R., McClintock, J. E., & Ebisawa, K. 2009, PASP, 121, 1279
- Tetarenko, A. J., Petitpas, G., Sivakoff G. R., et al. 2018, ATel #11831
- Trushkin, S. A., Nizhelskij, N. A., Tsybulev, P., G., & Erkenov, A. 2018, ATel #11439
- Tucker, M. A., Shappee, B. J., Holoien, T. W.-S., et al. 2018, ApJL, in press
- Uttley, P., Gendreau, K., Markwardt C., et al. 2018, ATel #11423
- Veledina, A., Poutanen, J., & Vurm, I. 2013, MNRAS, 430, 3196
- Veledina, A., Berdyugin, A. V., Kosenkov, I. A., et al. 2018, A&A, submitted (arXiv:1808.09002)
- Wang, S., Kawai, N., Shidatsu, M., et al. 2018, PASJ, 70, 67
- Wilms, J., Allen, A., & McCray, R. 2000, ApJ, 542, 914
- Yatsu, Y., Kawai, N., Shimokawabe, T., et al. 2007, *Physica E Low-Dimensional Systems and Nanostructures*, 40, 434
- Yu, W., Zhang, J., Yan, Z., Wang, X., & Bai, J. 2018, ATel #11510
- Zacharias, N., Finch, C. T., Girard, T. M., et al. 2013, AJ, 145, 44
- Zycki, P. T., Done, C., & Smith D. A. 1999, MNRAS, 309, 561